Asian Journal of Pharmaceutical Sciences 17 (2022) 268–283

Available online at www.sciencedirect.com

ScienceDirect

journal homepage: www.elsevier.com/locate/AJPS

Original Research Paper

Alantolactone-loaded chitosan/hyaluronic acid nanoparticles suppress psoriasis by deactivating STAT3 pathway and restricting immune cell recruitment

Ruijie Chen[a,†], *Yuan-Yuan Zhai*[b,†], *Lining Sun*[a], *Zeqing Wang*[b], *Xing Xia*[a], *Qing Yao*[b,*], *Longfa Kou*[a,*]

[a] *Department of Pharmacy, the Second Affiliated Hospital and Yuying Children's Hospital of Wenzhou Medical University, Wenzhou 325027, China*

[b] *School of Pharmaceutical Sciences, Wenzhou Medical University, Wenzhou 325035, China*

ARTICLE INFO

Article history:
Received 12 January 2022
Accepted 19 February 2022
Available online 27 February 2022

Keywords:
Psoriasis
Alantolactone
STAT3
Chitosan
Nanoparticle

ABSTRACT

Psoriasis is a common chronic immune-mediated skin disease characterized by hyperproliferation and aberrant differentiation of keratinocytes and massive infiltration of inflammatory immune cells. Recent studies showed that Signal Transducer and Activator of Transcription 3 (STAT3), which plays an important role in cell survival, proliferation, differentiation, angiogenesis, and immune responses, is constitutively activated in epidermal keratinocytes of human psoriatic skin lesions. In addition, STAT3 promotes the differentiation and expansion of T cells and facilitates cytokine production, thereby exacerbating the condition of psoriasis. Alantolactone (ALT) is a sesquiterpene lactone compound that could selectively suppress STAT3 activation, but its effectiveness and application in psoriasis treatment have not been determined. In this study, we developed ALT loaded chitosan/hyaluronic acid nanoparticles (CHALT), and investigated its therapeutic potential for psoriasis therapy. CHALT effectively abrogated the hyperproliferation by inducing ROS-mediated apoptosis with loss of mitochondrial membrane potential, and also inhibited IL-6-induced STAT3 signaling activation and inflammatory reaction in HaCaT cell line. In an Imiquimod (IMQ)-induced psoriasis model, the topical treatment of psoriasis lesions with CHALT effectively attenuated the STAT3 hyperactivation within keratinocytes and ameliorated the symptoms of psoriasis. In addition, it was found that CHALT restricted the recruitment of immune cells. These results indicated that ALT-based nanoformulation CHALT holds great potential for psoriasis therapy.

* Corresponding author.
E-mail addresses: yqpharm@163.com (Q. Yao), klfpharm@163.com (L.F. Kou).
† These authors contributed equally to this work.
Peer review under responsibility of Shenyang Pharmaceutical University.

https://doi.org/10.1016/j.ajps.2022.02.003

1. Introduction

Psoriasis is a chronic, immune-mediated, non-contagious skin disease. It is morphologically characterized by silvery scales, erythema, elevated thickness and formation of plaques, and pathological analysis further shows significant epidermal hyperplasia, dermal blood vessel formation, and lymph cell infiltration into the dermis [1]. The epidemiological study suggests that psoriasis is affecting approximately 2–3% of the worldwide population. Even though the etiology of psoriasis is still not well established, the risk factors, including hereditary, environmental, and deregulated immune system etc., were considered to be related [2,3]. Untreated psoriasis could progress to obesity, hyperlipidemia, arthritis, or cardiovascular diseases, significantly lowering the quality and even increasing mortality [4,5]. Current treatments for psoriasis include topical application of corticosteroids or vitamin D3 analogs, systemic administration of biological agents (like interleukin-17 inhibitor), and phototherapy [4,6]. However, due to nonadherent treatment schedules and poor patient compliance, none of these treatment strategies have been proven efficacious. Further investigations should be conducted to develop new, effective, and convenient therapeutic options.

Even though psoriasis' etiology has not been fully elucidated, Signal Transducer and Activator of Transcription (STAT) 3 an emerging key player in pathogenesis and development of psoriasis [7,8]. STAT3, one of the prominent members of STAT family, is a latent transcription factor. It plays a critical role in cell survival, differentiation, proliferation, angiogenesis, and immune activation. At psoriasis skin lesions, STAT3 was found to be notably upregulated in both keratinocyte and infiltrated lymph cells [9–11]. To be specific, STAT3 plays a crucial role in the signal transduction cascades of interleukin (IL)−6, IL-21, and IL-23 as well as the differentiation and expansion of T-helper type 17 (Th17) cells [12–16], which was considered as a culprit in psoriasis. Emerging evidence indicated that STAT3 is critical for the pathogenesis and development of psoriasis and could be an ideal target for psoriasis treatment. In our previous study, we have shown that alantolactone (ALT), a natural sesquiterpene lactone isolated from inula helenium, holds a potent inhibitory effect on the STAT3 pathway [17]. And here we would like to further develop an ALT-involved strategy and explore its potential for psoriasis therapy.

Nanocarriers have shown advantages for drug delivery over conventional systems, including controlled release, increased solubility and stability, and enhanced delivery efficiency [18–20]. For example, Pukale et al. reported lipid-polymer hybrid nanoparticles (LPNs) for clobetasol propionate delivery to treat psoriasis. The *in vivo* study showed that LPNs penetrated into the viable epidermis and dermis region and significantly improved psoriasis area severity index (PASI) score, reduced skin damage and proliferation [21]. Hyaluronic acid (HA) has specific interaction with CD44 on cell surface [22,23]. Based on the overexpressed CD44 in inflamed psoriatic skin, Zhang et al. developed a HA-conjugated and propylene glycol-based ethosomes to actively target CD44 in psoriatic skin for enhanced curcumin delivery for psoriasis treatment and found that this nanoparticle could increase the topical delivery of curcumin to inflamed skin and exert satisfactory therapeutic effect [24]. Recently, researchers found that cationic polymers could scavenge nucleic acids from dead and dying cells to destroy the immune complexes, thereby providing a new concept to treat inflammation [25]. Chitosan, a naturally occurring N-deacetylated derivative of chitin composed of mainly glucosamine units, has been widely explored as biodegradable biomaterials for drug delivery. Notably, chitosan is also a positively charged polymer and has been verified to hold anti-inflammation properties [26]. In addition, chitosan-based nanocarriers usually have positive potential, which provides electrostatic interaction with biological membranes, enhancing binding and transdermal drug delivery [27].

In this study, we prepared a chitosan/hyaluronic acid-based nanoparticle to deliver ALT (CHALT) for psoriasis treatment as indicated in Schematic 1. The physicochemical properties of CHALT were detailly characterized. CHALT could effectively abrogate the hyperproliferation by inducing ROS-mediated apoptosis with loss of mitochondrial membrane potential, and also inhibited IL-6-induced STAT3 signaling activation and inflammatory reaction in HaCaT cell line. Using an Imiquimod (IMQ)-induced psoriasis model, we demonstrated that the topical treatment of psoriasis lesions with CHALT nanoformulation effectively ameliorated the symptoms of psoriasis and restricted the recruitment of immune cells.

2. Materials and methods

2.1. Materials

Alantolactone was purchased from Chengdu Pufei De Biotech Co., Ltd (Chengdu, China). Chitosan, triphosphate (TPP) and hyaluronic acid were brought from Sigma-Aldrich (Saint Lious, MO, USA). Indocyanine green (ICG) (Catalog No. MB4675) was obtained from Meilunbio VR (Dalian, China). Fetal bovine serum (FBS), Dulbecco's Modified Eagle's Medium (DMEM), phosphate buffered saline (PBS) and trypsin were purchased from Life Technologies (Grand Island, NY). Phosphotungstic acid was obtained from Sinopharm Chemical Reagent Co.,Ltd (Shanghai, China). Hematoxylin and Eosin (H&E) staining kit, MASSON staining kit and Mitochondrial membrane potential Assay Kit were purchased from Solarbio (Beijing, China). The anti-Ki67 (ab 15,580) was obtained from Abcam (MA, US). Anti-CD8 (AF5126), Cytokeratin 10 (CK 10, AF0197), IL-6 (DF6087) were purchased from Affinity Biosciences (OH, USA). Anti-CD8 (bs-0648R) was purchased from Bioss. Anti-p-stat3 (D3A7), p-src (D49G4), STAT3 (D1B2J) and p-JAK2 (C80C3) were purchased from Cell Signaling Technology (MA, USA). β-actin (EM21002) was purchased from HuaAnbio company (Zhejiang, China). Anti-CD4 (bs-0647R) was obtained from BIOSS company (Beijing, China). The anti-PECAM-1 (sc365804) was obtained from Santa Cruz Biotechnology (TX, USA).

The HaCaT cells was obtained from the Fenghbio Co., Ltd (CL0114, Hunan, China). HaCaT were grown in DMEM medium with high glucose and 10% (v/v) FBS, cultured in a humidified 5% CO_2 incubator at 37 °C.

All animal experiments and study protocols were subjected to approval by the Animal Care and Use Committee of Wenzhou Medical University. BALB/c mice (4–6 weeks) were supplied by the Experimental Animal Center of Wenzhou Medical University. The animals were hosted in a controlled environment (25±2 °C, 12 h light/dark cycles, and 55%±5% relative humidity) with specific-pathogen-free condition.

2.2. Preparation of CHALT nanoparticles

Alantolactone loaded cross-linked chitosan/hyaluronic acid nanoparticles (CHALT) were prepared by a modified ionic gelation method using TPP as a crosslinker [9,28]. Firstly, chitosan was dissolved in 2% acetic acid solution to a concentration of 2 mg/ml before adjusting the pH to 4.0, and hyaluronic acid was dissolved in water (1 mg/ml). Then the hyaluronic acid solution and TPP solution were dropped into the chitosan solution, and the final solution was kept under continuous stirring at 500 rpm overnight. The final weight ratio of chitosan: TPP: hyaluronic acid in the formulation was 4:1:0.5. Alantolactone in DMSO (1 mg/ml) was added to blank chitosan/hyaluronic acid nanoparticle (CH) under continuous stirring for loading. The obtained solution was dialyzed (MWCO, 7000 Da) against water, and the final CHALT was achieved by lyophilization.

2.3. Characterization of CHALT nanoparticles

The mean particle size, polydispersity index (PDI), and zeta potential were determined by Zeta sizer Nano ZSP (Malvern Instruments, Ltd., Worcestershire, UK). The morphology of CH and CHALT nanoparticles was visualized by transmission electron microscope (TEM) (JEOL, JEM 1200EX, Japan). Negative staining using 1% phosphotungstic acid (Sinopharm Chemical Reagent, Shanghai, China) was performed for TEM study.

2.4. In vitro release assay

The *in vitro* release profile of alantolactone from nanoparticles was investigated using a dialysis method as we previously reported [17]. Briefly, ALT solution or CHALT were placed in a dialysis bag (MWCO, 3000 Da) and immersed in PBS (pH = 7.4) containing 1% tween 80 (v/v) under continuous shaking (100 rpm) at 37 °C. 2 mL of samples was collected at predefined intervals and replenished with same-volume of fresh medium. Then the samples were analyzed by an HPLC method as described in the following paragraph.

HPLC system of Agilent 1260 series was used. The mobile phase consisted of acetonitrile and formic acid solution (0.1%, v/v) with a volume ratio of 70:30. Isocratic elution was employed with a flow rate of 1.0 ml/min. The samples were diluted with methanol, filtered through a 0.45-μm nylon springe filter before injection (20 μl). The detection wavelength was settled at 220 nm. A Hanbon column (5 μm, 4.6 mm × 250 mm) was used for HPLC analysis with the column temperature maintained at 30 °C.

2.5. Cellular uptake studies

The cellular uptake assay was performed on HaCaT cells. ICG was used as a probe to indicate the uptake profile of nanoparticles. Briefly, HaCaT cells were seeded into 6-well plates at a density of 5×10^4 cells per well. After adhesion, the cells were incubated with 5 μg/ml of ICG or ICG-loaded CH. Following 1 h incubation, the cells were washed with cold PBS three times, and then visualized under a fluorescence microscope (Olympus Corp., Tokyo, Japan). For flow cytometry assay, the cells after washing were treated by trypsin for appropriate time for detachment. The cells were then collected and processed to make a single-cell suspension in a concentration of 1×10^7 cells/ml. The cells with ICG fluorescence were determined using a flow cytometry (Beckman Cytoflex).

2.6. MTT assay

MTT assay was conducted to investigate the effect of ALT and CHALT on the proliferation of HaCaT cells. Briefly, HaCaT cells were seeded in 96-well plate in a density of 5×10^3 cells/well. After 24 h, the cells were treated with various concentrations of ALT or CHALT and allowed for another 6, 12 or 24 h incubation. Following that, 10 μl of MTT solution (5 mg/ml) was added, and the plate was kept at 37 °C for an additional 3 h. Then remove the supernatant and add 150 μl DMSO to dissolve the formed formazan. The absorbance was measured at 492 nm.

To further investigate the anti-inflammation properties of CHALT, IL-6-induced inflamed HaCaT cell line was used as a cell model. Before treatments by CHALT, the cell inflammation was firstly induced by IL-6 (20 ng/ml) at 37 °C for 12 h. The following procedures were the same as described above.

2.7. Apoptosis study by flow cytometry

HaCaT cells were seeded into 6-well plates at a density of 1×10^6 cells per well and cultured for 24 h. Then, the cells were treated with ALT or CHALT at different concentrations. Following 3 or 6 h treatment, the cells were washed with PBS, trypsinized, and resuspended in binding buffer. The cells were then stained with Annexin V-FITC conjugate and PE according to the manufacturer's protocol. The samples were tested by flow cytometry (Cytoflex, Beckman Coulter, USA). The results were analyzed using FlowJo Version10 software.

2.8. JC-1 staining

Mitochondrial membrane potential ($\Delta\Psi$) was determined by JC-1 staining to investigate the effects of CHALT on mitochondrial polarization. In brief, HaCaT cells were seeded into 6-well plates containing coverslips at a density of 1×10^6 cells/well. After 24 h, the cells were treated with various concentrations of CHALT and incubated for another 6 h. Following that, cells on the coverslips were labeled with 10 μg/ml of JC-1 dye and DAPI. The stained cells were visualized by fluorescence microscope (Olympus Corp., Tokyo,

Table 1 – The sequence of primers used in this study.

Gene	Primer	Base sequence (5′ to 3′)
hTNF-α	Forward	CTGGGCAGGTCTACTTTGGG
	Reverse	CTGGAGGCCCCAGTTTGAAT
hIL-6	Forward	GTCCAGTTGCCTTCTCCCTGG
	Reverse	CCCATGCTACATTTGCCGAAG
hIL-17	Forward	TCTGTGATCTGGGAGGCAAAG
	Reverse	CCCACGGACACCAGTATCTTC
hIL-22	Forward	GGGAGAAACTGTTCCACGGAG
	Reverse	TGACATGTGCTTAGCCTGTTGC
hSTAT3	Forward	CTGTCAGATGCCAAATGC
	Reverse	CTTACCGCTGATGCCTT
hGAPDH	Forward	CCATGGGGAAGGTGAAGGTC
	Reverse	AGTGATGGCATGGACTGTGG

Japan). The quantitative analysis was performed using Image J software.

2.9. *Intracellular ROS determination*

2′,7′-dichlorofluorescein diacetate (DCFH-DA) was used to indicate the intracellular ROS content. Briefly, HaCaT cells (1×10^5 cells/well) were seeded in 6-well plates containing coverslips. After adhesion, the cells were treated with different concentrations of CHALT for another 3 or 6 h. The cells were then stained with DCFH-DA (10 μM) at 37 °C for 30 min. The samples were mounted using DAPI-contained ProLong Diamond Antifade Mountant. The staining was tested using a fluorescence microscope (Olympus Corp., Tokyo, Japan), and the quantitative analysis was performed using Image J software.

2.10. *Quantitative real-time polymerase chain reaction (qRT-PCR)*

Trizol was used to isolate the total RNA, and the concentration and purity of isolated RNA were measured by NanoDrop 2000 (ThermoFisher, Shanghai, China). Complementary DNA (cDNA) was reverse transcribed from total RNA samples using a ABScript II RT Master Mix kit (ABclonal, China). qRT-PCR samples were prepared using a commercial kit (Genious 2X SYBR Green Fast qPCR Mix, ABclonal, China) and determined by a lightCycler 480 Sequence Detector System (Roche, Switzerland). All kits were used according to the manufacturer's instructions. The primers used in the study are shown in Table 1.

2.11. *In vivo anti-psoriasis study of CHALT*

BALB/c mice (4–6 weeks) were used to develop the psoriasis model. 5% IMQ cream (SMSP Company Ltd., Sichuan, China) was topically applied onto the shaved back or ear daily for one week. Briefly, the IMQ-treated mice received topical administration by smearing CHALT or ALT onto their specific back or auricle site using cotton swabs. This procedure was repeated several times for sufficient dose. The PASI score was used to assess the severity of disease by erythema, infiltration or thickness, scaling and the extent of lesions as reported [3]. The parts were scored independently on a scale from 0 to 4, where 0 = no clinical signs, 1 = slight clinical signs, 2 = moderate clinical signs, 3 = marked clinical signs, and 4 = very marked clinical signs.

Experimental mice were randomly divided into five groups ($n = 3$), and one group was selected as a health control. The mice in the other four groups were applied by IMQ to induce psoriasis. Following IMQ application, the mice were also treated by ALT (30 μM), CHALT (20 μM), and CHALT (30 μM) once daily in one week. The operation was same as described above. The group without further treatment was used as a model group. During treatments, the PASI score and mouse weight was recorded every day. After 7 d, the mice were sacrificed, and the skin samples of identical areas and spleens were collected. The skin samples were used for histological analysis. The spleens were weighted and also used for immune analysis. The weight ratio of spleen/body was calculated to indicate the immune stimulation or depletion.

2.12. *Histopathological examination of skin and ear tissues*

Fresh ear or back skin samples were fixed, dehydrated, cleared and embedded into paraffin wax. The samples were then sliced into pieces (5 μm) and prepared onto slides. H&E and Masson staining were used to examine histological morphology. Immunohistochemistry (IHC) was used to detect the levels of CK 10 (Affinity, China) and Ki 67 (Abcam, USA). Immunofluorescence staining was conducted to evaluate the activation of immune cells in IMQ-induced skin. Images were captured using a microscope (Olympus Corp., Tokyo, Japan). Quantitative analysis was conducted using Image J software.

2.13. *Western blot analysis*

Cells and skin tissue were collected and lysed as previously reported [29–31]. The protein concentration was quantified using a BCA kit (Beyotime, China). Equal amounts of proteins were separated by sodium dodecyl sulfate-polyacrylamide gel electrophoresis (SDS-PAGE) on a 12% gel and transferred to a polyvinylidene difluoride membrane. The membranes were blocked using 5% skim milk for 1 h, and then incubated with primary antibodies at 4 °C overnight. After proper washing, the membranes were further incubated with horseradish peroxidase (HRP)-conjugated secondary antibodies (MULTI SCIENCES, China) for 1 h. At last, proteins were detected using an ECL kit and an automatic chemiluminescence image analysis system. Quantitative analysis was performed using Image J software.

2.14. *Statistical analysis*

Data were analyzed using GraphPad Prism Version 8.0 software. Statistical differences between groups were calculated with Student's *t*-test or one-way analysis of variance. Data are shown as mean ± SD. $P < 0.05$ was considered statistical significance.

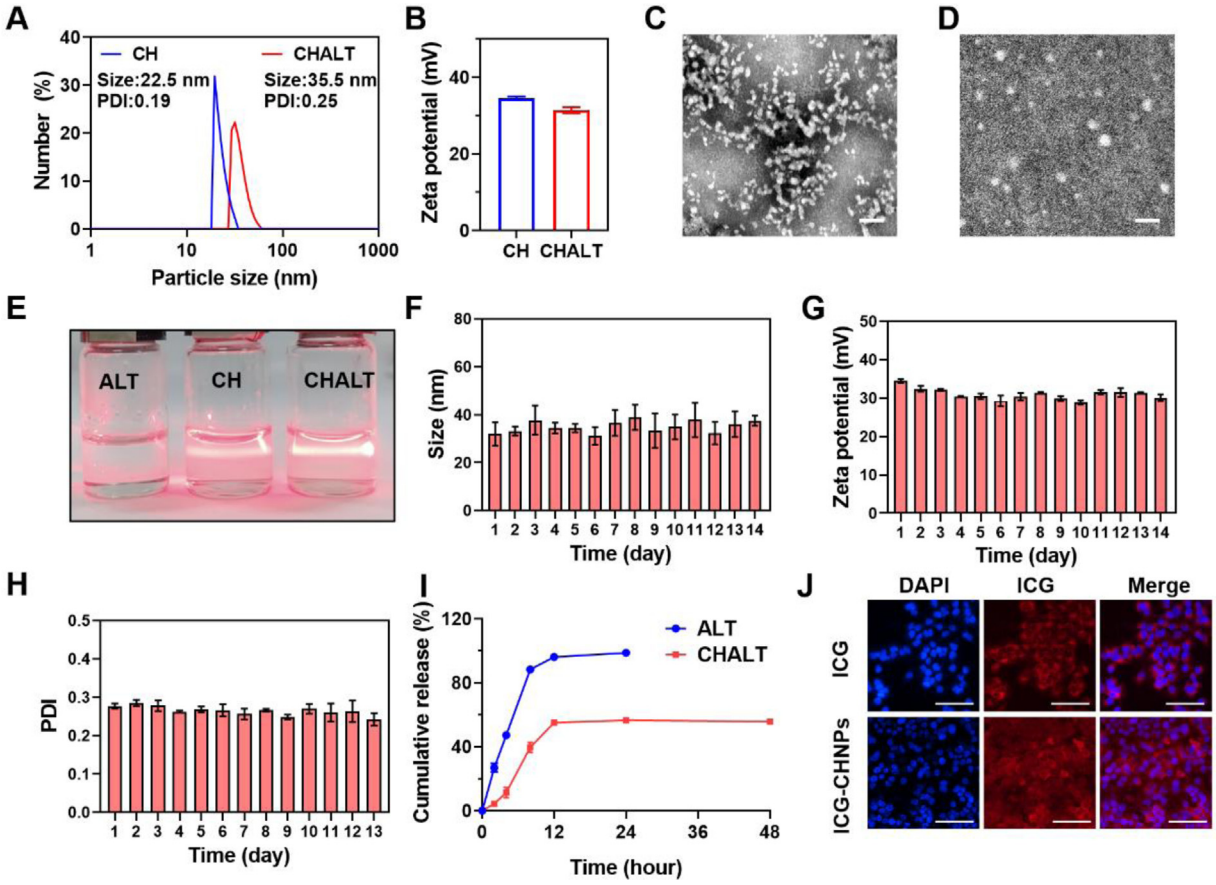

Fig. 1 – Characterization and cellular uptake profile of CHALT nanoparticles. (A) The hydrodynamic size and (B) zeta potential of CH blank nanoparticles and CHALT nanoparticles. TEM images of (C) CH and (D) CHALT nanoparticles (Scale bar = 50 nm). (E) Photograph shows the Tyndall effect in solutions with different compositions: left: ALT dissolved in DMSO, middle: CH nanoparticles in water, right: CHALT nanoparticles in water. The stability of CHALT in two weeks was measured, and (F) the size, (G) zeta potential and (H) PDI were monitored daily ($n = 3$). (I) Cumulative ALT release from ALT solution or CHALT nanoparticles in pH 7.4 PBS containing 1% tween 80 at 37 °C ($n = 3$). (J) Cellular uptake of ICG-loaded nanoparticles by HaCaT cells *in vitro*. (Blue: nucleus; Red: ICG; Scale bar: 100 μm). (For interpretation of the references to colour in this figure legend, the reader is referred to the web version of this article.)

3. Results and discussion

3.1. *Preparation and characterization of CHALT*

CHALT nanoparticles were prepared by ionic gelation of chitosan and hyaluronic acid. The particle size of CHALT was characterized by a dynamic light scattering method. As shown in Fig. 1A, CH had a particle size peak around 22.5 nm. ALT loading increased the nanoparticle size up to 35.5 nm. The polydispersity indexes (PDI) of CH and CHALT were 0.19 and 0.25, respectively. The low PDI values indicated the narrow distribution of CH and CHALT. The zeta potential of CH and CHALT was 34.5 ± 0.8 mV and 31.4 ± 0.7 mV, respectively (Fig. 1B). TEM images showed that both CH and CHALT have a spherical shape (Fig. 1C and 1D), and CHALT is slightly bigger than CH, which is consistent with the DLS results. In addition, the Tyndall effect test was performed to identify the dispersity of nanoparticles. As shown in Fig. 1E, a laser beam was forced to go through ALT solution, CH nanoparticles and CHALT nanoparticles. A manifest beam path was observed in both CH and CHALT nanoparticles, but none in ALT solution, indicating the good dispersity of both CH and CHALT nanoparticles. Collectively, these results indicated the successful preparation of ALT-based nanoparticles CHALT with a small average size and narrow distribution.

The colloidal stability of CHALT was further investigated. We monitored size (Fig. 1F), zeta potential (Fig. 1G), and PDI (Fig. 1H) of CHALT nanoparticles every day within two weeks, and no significant changes in aggregation or sedimentation were observed, indicating a satisfying stability. An HPLC method was developed to quantify ALT concentration to calculate the encapsulation efficiency (EE) and drug load (DL) of ALT in nanoparticles, as well as the *in vitro* release profiles of ALT from nanoparticles. As shown in Fig. S1A, the HPLC curve showed that the peak of ALT has good specificity and the retention time is 10.242 min. The calibration curve ranging from 2.5 to 100 μg/ml has good linearity ($R^2 = 0.9929$) (Fig. S1B). Based on this HPLC method, the EE and DL of ALT in CHALT were determined as 85.21%±3.46% and 4.06%±0.16%, respectively. A dialysis method was conducted to assess the release characteristics of ALT from CHALT in pH 7.4 PBS

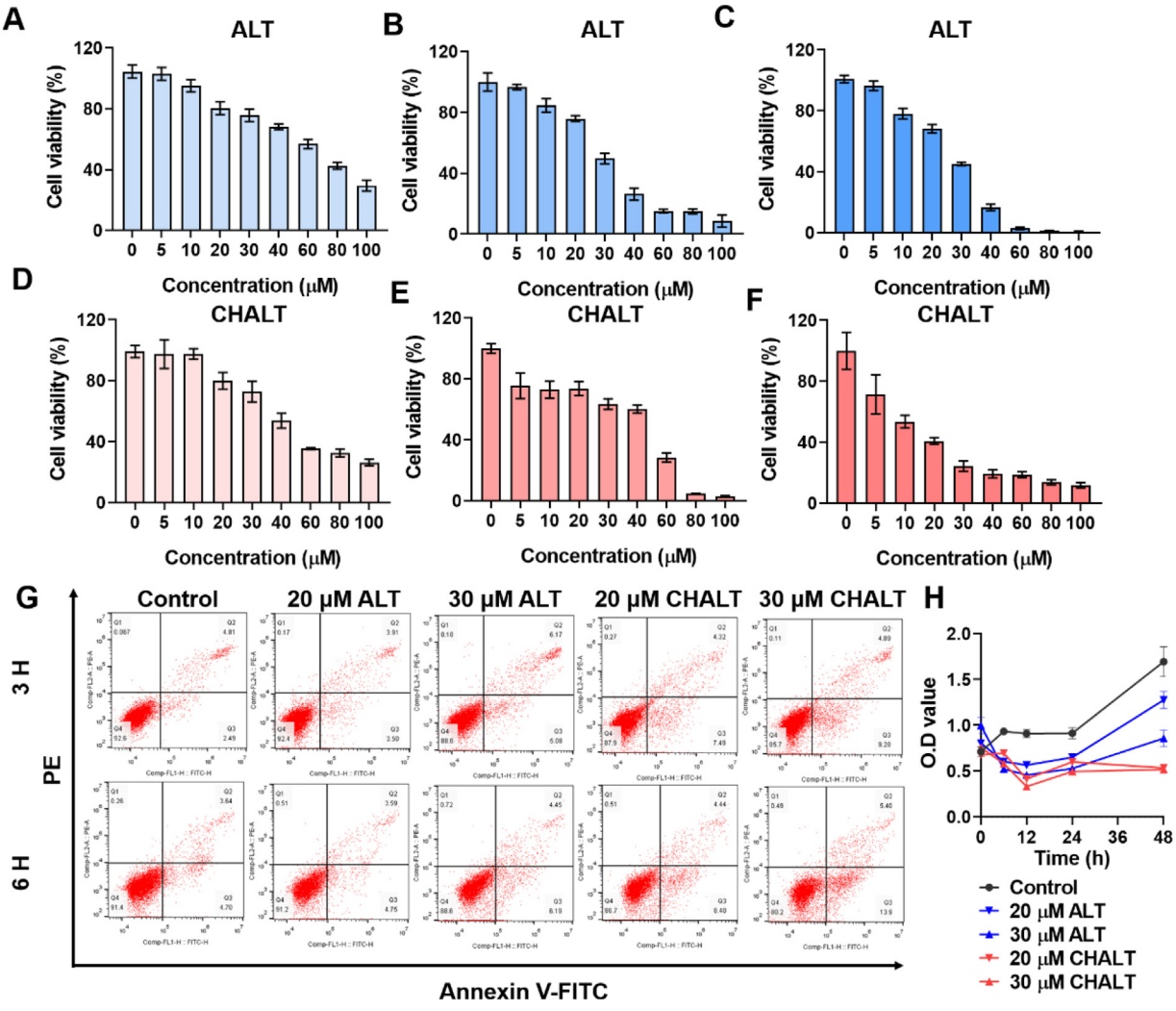

Fig. 2 – CHALT inhibited the proliferation of HaCaT cells by inducing apoptosis. The cell viability of HaCaT after ALT treatment with various concentrations for (A) 6 h, (B) 12 h and (C) 24 h. The cell viability of HaCaT after CHALT treatment with various concentrations for (D) 6 h, (E) 12 h and (F) 24 h ($n = 6$). (G) Apoptosis analysis of HaCaT cells after treatment by ALT (20 μM), ALT (30 μM), CHALT (20 μM), and CHALT (30 μM) for 3 h (top) or 6 h (down). (H) The HaCaT cell viability after treatment by ALT (20 μM), ALT (30 μM), CHALT (20 μM), and CHALT (30 μM) for 6, 12, 24, and 48 h ($n = 6$).

containing 1% tween 80. As shown in Fig. 1I, free ALT showed a very fast release, and the cumulative release was up to ~90% in the first 12 h. In comparison, CHALT displayed a distinct sustained manner, which was a benefit for the setting of chronic disease like psoriasis, as it avoids frequent, repeated administration. Thus, the prepared CHALT nanoparticles have desirable colloidal stability and the ALT could be slowly released from the nanoparticles.

The positively charged surface potential could facilitate nanoparticle binding and internalize into cells, and then promote the transdermal drug delivery efficiency [32]. Therefore, we investigated the uptake profiles of CHALT in HaCaT cells using ICG as a fluorescence probe (Fig. 1J), and the quantitative analysis was shown in Fig. S2. After incubation, clear red fluorescence was observed in both free ICG and ICG-loaded CH nanoparticle groups. Whereas, ICG-CH nanoparticles showed a stronger signal than free ICG, indicating the enhanced uptake of CH nanoparticles. This result was further confirmed by the flow cytometry (Fig. S3), in which ICG-CH nanoparticles presented stronger signal compared to free ICG. Positive potential-mediated enhanced binding and nanoparticle-mediated endocytosis might contribute to this phenomenon [33]. These results suggested that the CH nanoparticles prepared here were suitable for topical drug delivery.

3.2. *CHALT suppressed keratinocyte hyperproliferation by inducing apoptosis*

The persistent keratinocyte proliferation and evasion of apoptosis signals have been considered as hallmarks of psoriasis. HaCaT cells are a type of cells that spontaneously immortalized from a primary culture of keratinocytes. Herein, we used HaCaT cells as a model system to study the effect of CHALT on the *in vitro* events of keratinocyte proliferation in psoriasis. As shown in Fig. 2A-2C, with the increase of

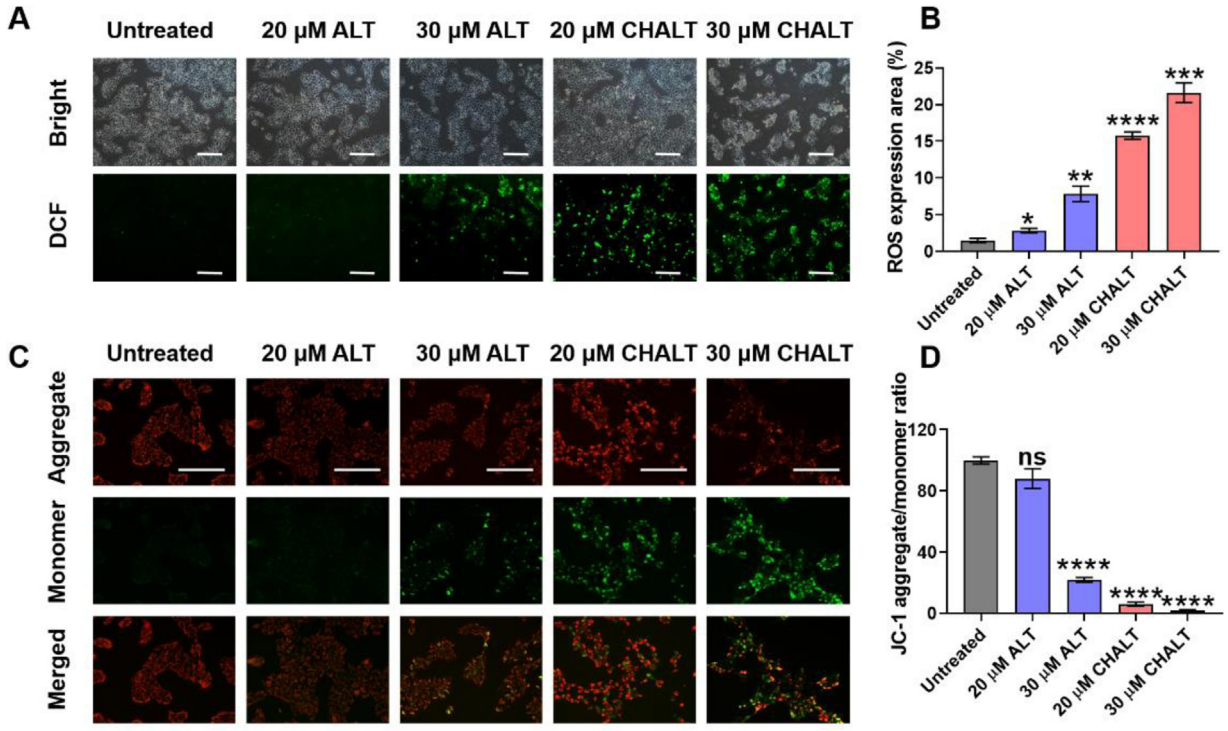

Fig. 3 – CHALT nanoparticles induce ROS production and mitochondrial membrane potential reversion in HaCaT cells. (A) Fluorescent images showed ROS production (DCF: green) by ALT or CHALT treatment (scale bar = 100 μm). (B) Relative ROS production in each group ($n = 3$). (C) JC-1 staining indicating the mitochondrial membrane potential (monomer: green; aggregate: red) (scale bar = 100 μm). (D) Quantitative JC-1 aggregate/monomer ratio ($n = 3$). *$P < 0.05$, **$P < 0.01$, ***$P < 0.001$, ****$P < 0.0001$, indicate statistical difference compared to the untreated group, and ns indicates no statistical significance. (For interpretation of the references to colour in this figure legend, the reader is referred to the web version of this article.)

ALT concentration, the cell viability of incubated HaCaT was decreased, indicating a dose-dependent manner. With the treatment time increased from 6 h to 24 h (Fig. 2A-2C), the HaCaT viability was further decreased, indicating a time-dependent manner. CHALT showed a similar trend as ALT (Fig. 2D-2F). These results suggested CHALT exerted a significant anti-proliferation effect on keratinocytes *in vitro* with a dose- and time-dependent manner and loading into a CH nanosystem would not interfere with the therapeutic effect of ALT. The comparison in suppressing keratinocyte proliferation between ALT and CHALT showed that CHALT hold stronger capacity compared to ALT in most cases, indicating the improved performance of ALT after loading into CH nanoparticles (Fig. S4). Based on these results, we further studied the apoptosis condiction of HaCaT cells after incubation with ALT or CHALT using flow cytometry (Fig. 2G). As is shown, after 3 h treatment, 30 μM ALT could increase the apoptotic rate (Annexin V-FITC-positive) from 7.30% to 11.25%, and 30 μM CHALT could increase the apoptotic rate up to 14.17%. After 6 h treatment, 30 μM CHALT could further increase the apoptotic rate up to 19.30%. The increased suppressing keratinocyte proliferation and pro-apoptosis property of CHALT in comparison to isodose ALT might be due to the enhanced uptake of CHALT (Fig. 1J and S3). Furthermore, we monitored the proliferation of HaCaT cells after treatment with ALT and CHALT in 48 h using MTT assay. As shown in Fig. 2H, ALT inhibited cell proliferation to some extent, and CHALT of both 20 μM and 30 μM showed a stronger effect, which was consistent with the apoptosis assay. These results suggested that CHALT could exert a remarkable inhibitory effect on the keratocyte proliferation by inducing apoptosis.

Reactive oxygen species (ROS) play an important role in the regulation of cell proliferation and apoptosis. In the early stages of apoptosis, a distinctive feature is the disruption of active mitochondria, which includes mitochondria membrane potential changes and ROS accumulation [34]. These two factors synergistically promote apoptosis [35]. In addition, it has been reported that ALT could increase ROS level to a threshold in the cancer cells and induce cell death. Therefore, we hypothesized that CHALT induced cell apoptosis is associated with the over-production of ROS and mitochondria destruction. Thus, we studied the changes in ROS production and mitochondrial potential in HaCaT cells after CHALT incubation (Fig. 3). The fluorescent probe DCFH–HA was used to detect ROS. As shown in Fig. 3A, ALT treatment significantly enhanced the green signal in HaCaT cells, indicating the overproduced ROS production. It should be noted that at the same dose, the ALT nanoformulation, CHALT, boosted more ROS production as compared to the naked drug, ALT. 20 μM CHALT even induced higher ROS production than 30 μM the naked ALT. These results indicated that encapsulating ALT into a CH nanoparticulate system further enhance the drug action of ALT. Quantitative analysis confirmed these results (Fig. 3B). Following that, JC-1 staining was used to

investigate mitochondria potential alterations. As shown in Fig. 3C-3D, untreated cells showed clear red fluorescence (JC-1 aggregation) and negligible green (JC-1 monomer) signal, indicating the standard mitochondria membrane potential. After treatment by ALT or CHALT, green fluorescence appeared, and the ratio of red/green decreased, indicating mitochondrial depolarization. These results were consistent with the ROS production. The superior performance on ROS production and mitochondrial depolarization by CHALT might be attributed to the enhanced uptake of CHALT in comparison with ALT (Fig. 1J and S3). In addition, considering the critical role of ROS and mitochondrial disruption in apoptosis, these results jointly confirmed our hypothesis that ROS and mitochondrial destruction involved in the ALT induced apoptosis and helped to explain the increased apoptotic rate of CHALT treated HaCaT cells above, indicating a good therapeutic potential of CHALT for psoriasis.

3.3. *CHALT suppressed inflammation via inhibiting STAT3 signaling*

Recent studies have shown that the STAT3 pathway is a key factor in the pathogenesis and development of psoriasis, especially in the signal transduction cascades of IL-6, IL-21, and IL-23 as well as the differentiation and expansion of T-helper type 17 (Th17) cells [36–39]. Previous studies reported by our group and other investigators showed that ALT holds a potent inhibitory effect on the STAT3 pathway [17,40-43]. In this study, we developed ALT based nanoparticle (CHALT) and evaluated its therapeutic potential for psoriasis treatment for the very first time. To investigate the *in vitro* anti-psoriasis properties of CHALT, we used IL-6-stimulated HaCaT as an inflamed cell model [44]. We firstly monitored the proliferation of inflamed HaCaT cells by MTT assay (Fig. 4A). IL-6 stimulation (20 ng/ml) significantly increased the cell viability. When ALT or CHALT was applied, the cell viability was decreased back to the normal level. CHALT showed a stronger inhibitory effect than free ALT, which was consistent with the above results. We further determined the gene expression of inflammatory cytokines (including TNF-α, IL-6, IL-17, and IL-22) and STAT3 using Q-PCR (Fig. 4B-4F). As expected, IL-6 promoted the mRNA expression of these four inflammatory cytokines, whereas CHALT decreased their elevated expression, and the same concentration of ALT showed an attenuated effect. The superior inhibitory effect of CHALT could be attributed to the enhanced uptake (Fig. 1J and S3) and prolonged release profile (Fig. 1I). As for STAT3, IL-6 exposure upregulated the mRNA expression, but ALT and CHALT did not show a significant suppressing effect. The probable reason should be ALT did not affect STAT3's mRNA expression, but inhibit its phosphorylation. STAT3 activation is involving the phosphorylation of a critical tyrosine residue (Tyr705), then resulting in homo- or hetero-dimerization of STAT3, following enabling nuclear localization and DNA binding. This triggered the downstream gene transcription, including TNF-α, IL-6, IL-17, and IL-22. This could explain that ALT and CHALT changed the mRNA level of inflammatory cytokines but not for STAT3. Therefore, we further investigated the STAT3 phosphorylation of inflamed cells after treatment with ALT or CHALT using immunoblot assay. As shown in Fig. 4G and 4I, IL-6 stimulation increased p-STAT3 level, and ALT (30 μM) and CHALT (20 μM and 30 μM) receded this trend. Nevertheless, 20 μM ALT exerted negligible effect, which might be due to the insufficient intracellular dose. This result was consistent with the weak impact of 20 μM ALT on mRNA levels of inflammatory cytokines (Fig. 4B-4E). 20 μM CHALT generated sufficient inhibitory effect, even stronger than 30 μM ALT. This could be explained by the enhanced uptake and prolonged action of CHALT. In addition, we further determined the activation of upstream SRC [45], and the results showed that CHALT also exerted significant inhibitory effect on the phosphorylation of SRC (Fig. 4G and 4H). These results suggested ALT could block the activation of both SRC and STAT3, and CHALT could strengthen the effects via enhanced uptake and prolonged-release (Fig. 4J).

3.4. *CHALT attenuated IMQ-induced psoriasis severity in mice*

Imiquimod (IMQ), a TLR7/8 ligand and potent immune activator, was used here to induce and exacerbate psoriasis according to a reported method [46], and we used this model to investigate the therapeutic efficacy of CHALT against psoriasis (Fig. 5). The experimental design was shown in Fig. 5A. The appearance of the psoriatic back was recorded on Day 7 (Fig. 5B). Distinct scaly and thickened skin was observed on the model back, indicating the psoriasis-like skin formed. Due to the weaker efficacy *in vitro* study, we removed the group of 20 μM ALT. 30 μM ALT and 20 μM CHALT showed improved symptoms, but there were still clear scaling and erythema on the mouse back. 30 μM CHALT was able to improve the erythema with reduced wrinkles and skin thickness in IMQ-exposed skin, indicating a satisfactory therapeutic efficacy. PASI scores over time were recorded to indicate the severity of psoriatic skin lesions. As shown in Fig. 5C-5E, the condition of skin desquamation, scaling, and erythema in five groups was scored, and the total PASI score was calculated (Fig. 5F). The skin desquamation, scaling, and erythema in each group increased with time in the first four days. For scaling and erythema, a comparable low increase rate was observed in treatment groups; 30 μM CHALT even induced a slight decrease in desquamation and scaling. From the fifth day, all indexes in all treatment groups started to going down, but the extent was different. 30 μM CHALT showed the strongest ability to lower these indexes, while 20 μM CHALT also showed beneficial effects in the management of desquamation and erythema to some extent. On Day 7 (Fig. 5G), the PASI scores suggested that 30 μM CHALT significantly attenuated IMQ-induced psoriasis severity, very close to the normal condition. 30 μM ALT and 20 μM CHALT also showed therapeutic efficacy to some extent, and 20 μM CHALT even had a better performance than 30 μM ALT. Histological analysis by H&E staining (Fig. 5H) and quantitative analysis of the skin thickness (Fig. S5) further confirmed these results.

In addition, we also constructed the psoriasis-like skin on mouse ears and determined the treatment efficacy of CHALT and ALT using the ear model. As shown in Fig. S6, the ear appearance of all groups was photographed at Day

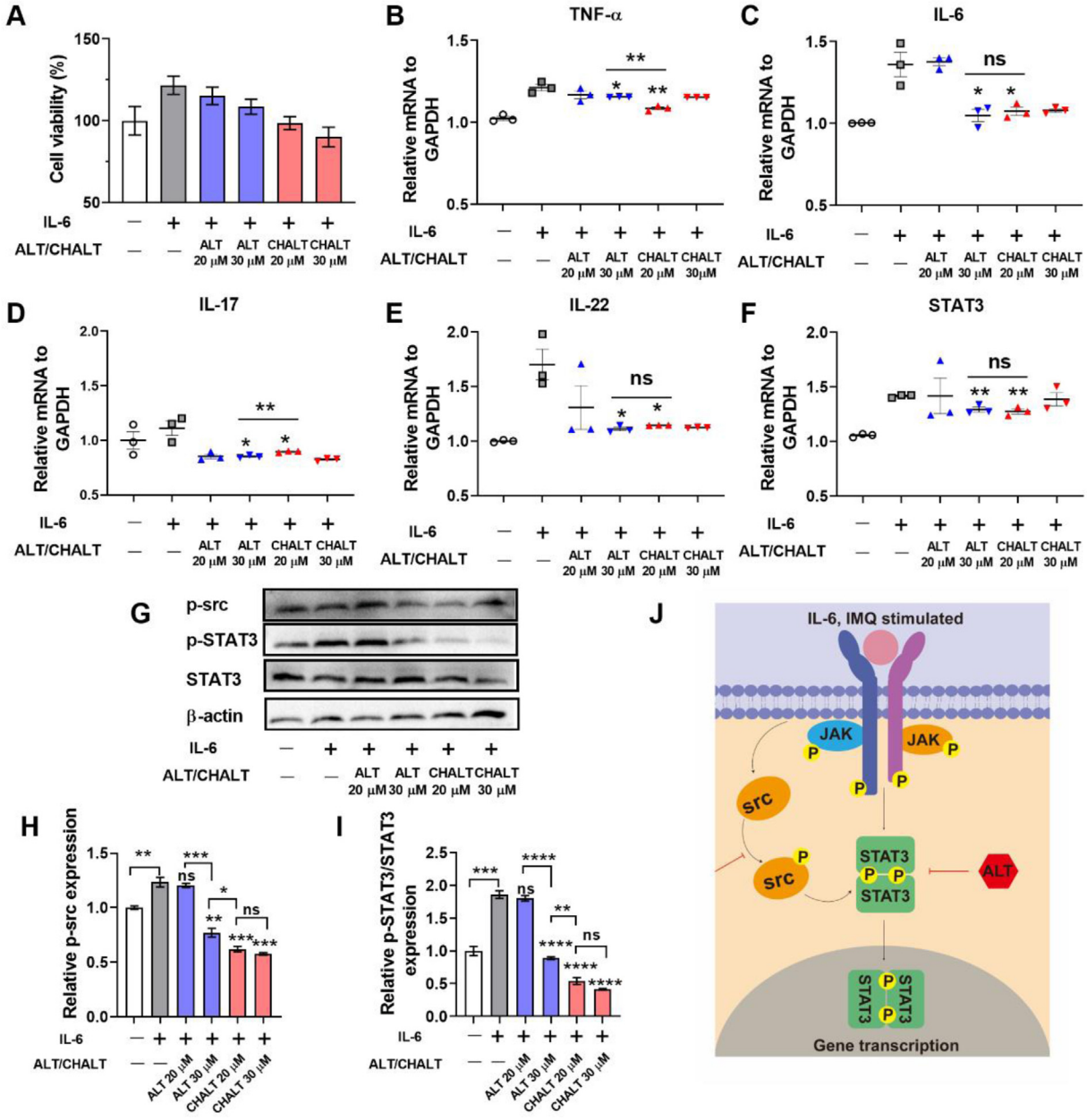

Fig. 4 – CHALT suppresses inflammation by inhibiting STAT3 phosphorylation *in vitro* studies. (A) MTT assay was performed to determine the cell viability of HaCaT after pretreated with IL-6 and then treated by ALT or CHALT ($n = 6$). RT-PCR was performed to study the mRNA expression of (B) TNF-α, (C) IL-6, (D) IL-17, (E) IL-22, (F) STAT3 after ALT/CHALT treatment, and GAPDH was served as an internal reference ($n = 3$). (G) Western blots show the expression of p-src, p-STAT3 and STAT3 proteins. Quantitative analysis of (H) p-src and (I) p-STAT3/STAT3 ($n = 3$). (J) Schematic diagram of CHALT/ALT inhibiting STAT3 phosophorylation in HaCaT cells. *P < 0.05, **P < 0.01, ***P < 0.001, ****P < 0.0001, indicate statistical difference compared to IL-6-treated group or between groups. ns indicates no statistical significance. (For interpretation of the references to colour in this figure legend, the reader is referred to the web version of this article.)

7, and H&E staining was performed to show the histological condition after the 7-d treatment. The IMQ-treated ear showed obvious desquamation, and histological analysis indicated thickening of the stratum corneum (evidenced by the quantitative analysis in Fig. S6B). 30 μM CHALT ameliorated IMQ-induced psoriatic phenotype to the best extent, and 20 μM CHALT also showed better efficacy than 30 μM ALT, which was consistent with the results on psoriatic back. The recorded PASI scores over 7 d on ears further confirm these results (Fig. S7). At that point, it was demonstrated that CHALT could effectively attenuate IMQ-induced psoriasis, and CHALT nanoparticle loading enhanced the therapeutic efficacy of ALT, indicating the potential of CHALT for anti-psoriasis application. The enhanced uptake and prolonged

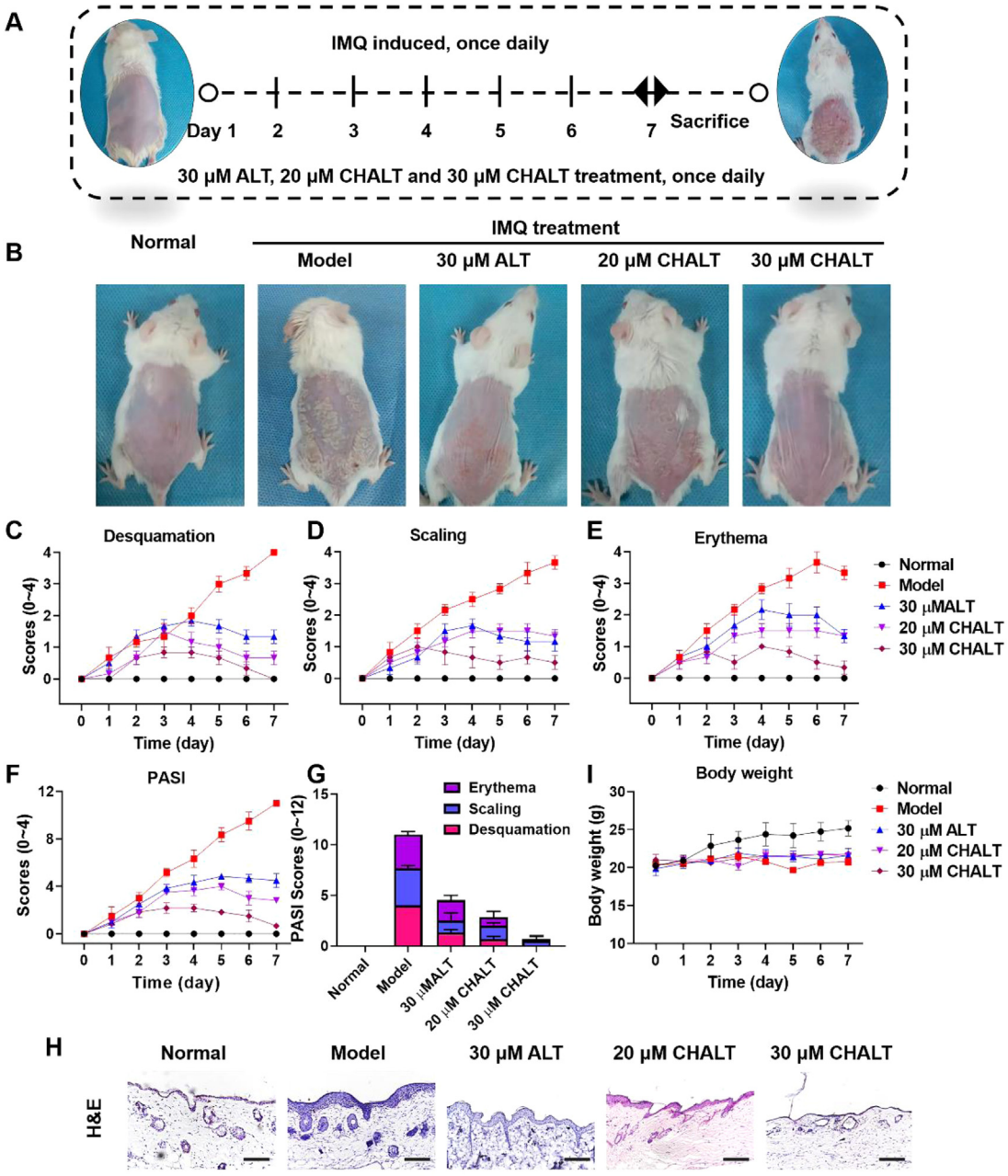

Fig. 5 – CHALT ameliorated IMQ-induced psoriasis in mice model. (A) The experimental design. (B) The macroscopic appearance of mouse back skin on Day 7. PASI score was monitored to quantify the disease severity by (C) desquamation, (D) erythema, and (E) scaling, and (F) the total PASI score were calculated. (G) The PASI score of all groups on Day 7. (H) H&E staining of back skin (scale bar = 100 μm). (I) Body weight changes in 7 d . (For interpretation of the references to colour in this figure legend, the reader is referred to the web version of this article.)

release properties of CHALT should be the reasons for the enhanced treatment outcome. Furthermore, improved skin penetration and prolonged retention time by positive-charged nanoparticles might also contribute to superior performance [27]. We also monitored the body weight in 7-d treatment. As shown in Fig. 5I, the body weight of mice in the model group decreased a little, and all treatment groups kept steady, indicating the safeness of CHALT and treatment retrieving psoriasis mice weight loss.

3.5. *Insights into the in vivo anti-psoriasis mechanisms of CHALT*

Hyperproliferation and aberrant differentiation of keratinocytes are crucial pathological changes in psoriasis. Therefore, we further investigated the effect of CHALT on psoriatic keratinocyte proliferation after 7-d treatment. Keratins are the intermediate filament proteins responsible for the structural integrity of epithelial cells, and Masson

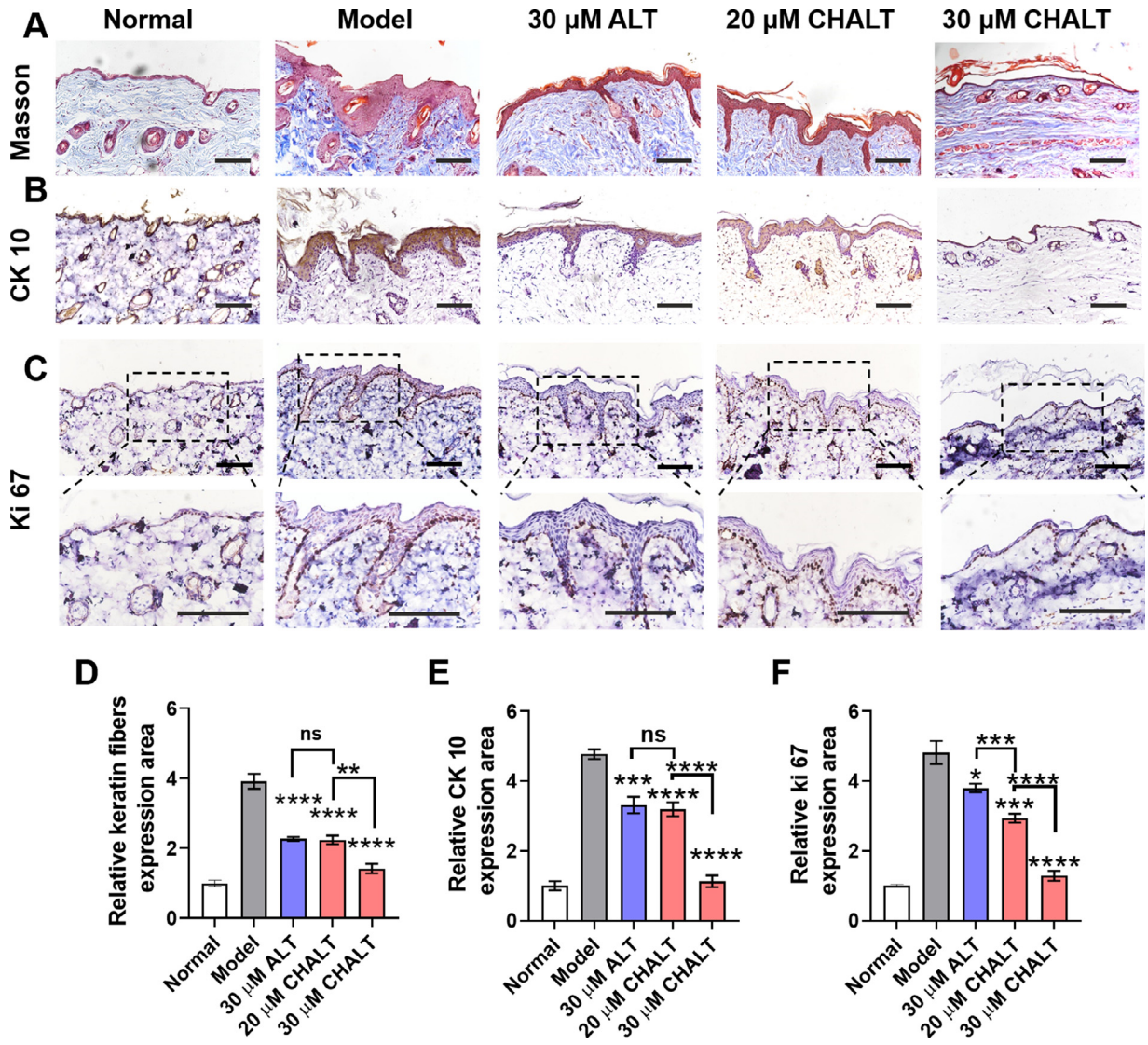

Fig. 6 – CHALT suppresses keratinocyte proliferation in IMQ-induced skin. The skin was evaluated by (A) Masson's trichrome staining, and quantitative analysis was shown (D). Immunohistochemical staining of (B) CK10 and (C) Ki 67 was performed, and quantitative analysis was shown in (E) and (F), respectively. Scale bar: 100 μM. *P < 0.05, **P < 0.01, ***P < 0.001, ****P < 0.0001, indicate statistical difference compared to model group or between groups. ns indicates no statistical significance. (For interpretation of the references to colour in this figure legend, the reader is referred to the web version of this article.)

staining was conducted to indicate keratin fibers to show the skin hyperproliferation (Fig. 6A). IMQ boosted the expression of keratin fiber in HaCaT cells, while ALT and CHALT could largely suppress this increase. Quantified analysis suggested that 30 μM ALT and 20 μM CHALT showed a similar inhibitory effect, while 30 μM CHALT remarkably decreased keratin fiber level, close to the normal (Fig. 6D). Cytokeratin 10 (CK10), a type I cytoskeletal keratin, was also determined to show the proliferation state of keratinocytes (Fig. 6B and 6E). The results were consistent with the Masson staining. Ki 67, a cellular marker for proliferation, was used as a cellular marker here to indicate epidermal hyperproliferation in psoriasis. As shown in Fig. 6C, Ki 67 expression in the model group was observably increased along with the thickened basal layer of the epidermis; in contrast, ALT or CHALT decreased Ki 67 expression in psoriatic skin. 30 μM CHALT still showed the strongest ability to suppress Ki 67 expression. What is interesting is that 20 μM CHALT showed a similar ability to inhibit keratin fiber and CK10, but hold a stronger ability to suppress Ki 67 expression. These results indicated that the dose of 20 μM CHALT was insufficient, and 30 μM CHALT was more suitable for psoriasis treatment.

Besides keratinocyte hyperproliferation, angiogenesis is also one of the significant features of psoriasis [47], and prominent dilation of the dermal blood vessels have been observed in different phases of psoriasis [48]. Here, we further studied the vascular alterations to further understand the therapeutic effect of CHALT. As shown in Fig. 7A, after 7-d induction by IMQ, the dermal blood vessels were dilated,

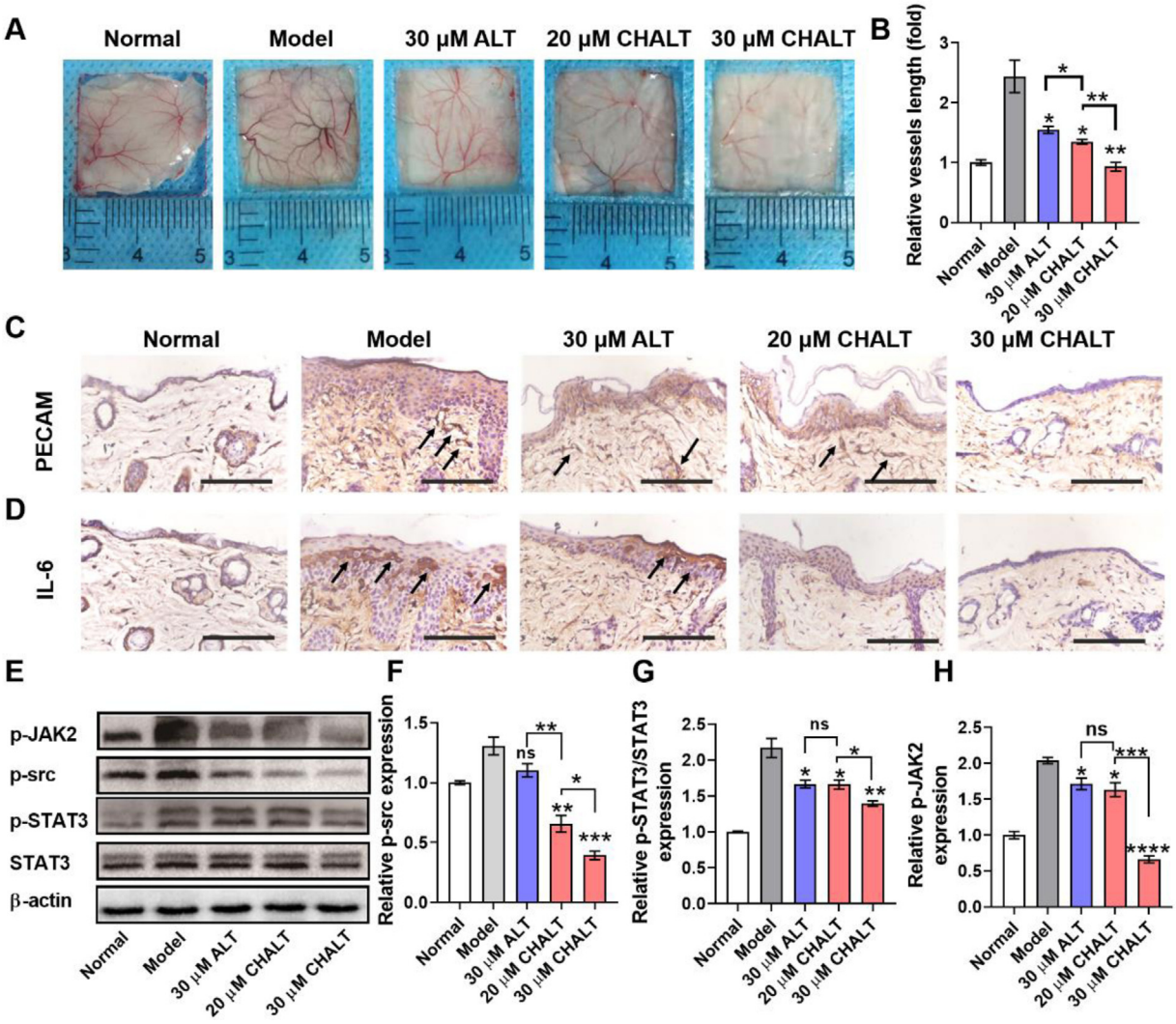

Fig. 7 – CHALT treatment ameliorates angiogenesis, inflammation, and inhibits STAT3 phosphorylation. (A) Phenotypical presentation and (B) vessels branches of dermal vessels in the mouse back skin after 7 d of treatment. Immunohistochemical assays of PECAM (C) and IL-6 (D) in the skin, scale bar = 100 μm. (E) Western blot assay of each group in p-src, p-STAT3, p-JAK2 and STAT3 expression *in vivo*, and relative expression of p-src (F), p-STAT3 (G) and JAK2 (H) in five groups were quantified (*β*-actin as the internal control). *P < 0.05, **P < 0.01, ***P < 0.001, ****P < 0.0001, indicate statistical difference compared to model group or between groups. ns indicates no statistical significance. (For interpretation of the references to colour in this figure legend, the reader is referred to the web version of this article.)

and new branched vessels were formed in the model group. As expected, ALT or CHALT treatment reduced the neovascularization in the psoriatic lesions to some extent. The vessel length was further quantified (Fig. 7B). It was shown that the vessel length in the group of 30 μM CHALTs decreased back to the normal level, indicating the strongest inhibitory effect and sufficient efficacy. 30 μM ALT and 20 μM CHALT also reduced psoriatic vessel length, but the effect was not up to that of 30 μM CHALT. The probable reasons might be the skimpy absorption of ALT or the insufficient dose of CHALT (20 μM). In addition, we also determined the expression of PECAM, a biomarker for endothelial cells in blood vessels [49], using an immunohistochemistry assay (Fig. 7C). A strong signal was observed in the model sample, and ALT or CHALT treatment decreased PECAM expression. Quantitative analysis indicated that 30 μM CHALT decreased PECAM expression back to normal level (Fig. S8A), and 30 μM ALT and 20 μM CHALT showed similar effect, consistent with the data in Fig. 7B. These results suggested CHALT attenuated psoriasis by suppressing angiogenesis, and CH nanoparticle loading could amplify the anti-psoriasis property of ALT.

IL-6 has been regarded to be involved in the development of psoriasis and is usually upregulated in psoriatic lesions [36,50]. IL-6 inhibitors or antagonists have been studied for psoriasis treatment [51]. The increased expression of IL-6 was also observed in our results (Fig. 7D and S8B). IMQ exposure induced distinct upregulation of IL-6, whereas ALT an CHALT showed an effective inhibitory effect, and 30 μM CHALT even decreased IL-6 expression to a normal level. These results

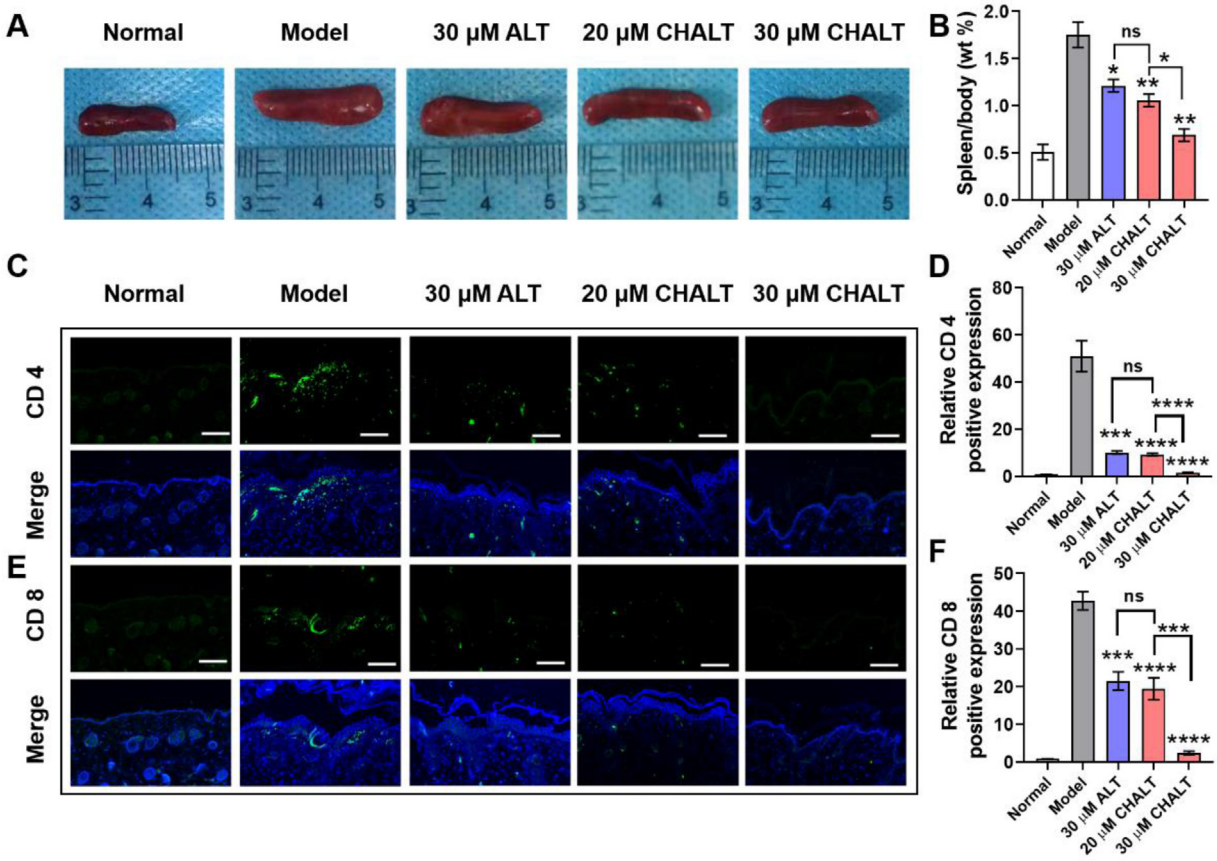

Fig. 8 – CHALT attenuates splenomegaly and immune cell recruitment in IMQ-induced skin. On Day 7, (A) the spleens were collected and photographed, and (B) the weight ratio of spleen/body was calculated. Immunfluorescence staining of (C) CD 4 and (E) CD 8 in the skin, and the relative amount of (D) CD 4 and (F) CD 8 was quantified (the normal group as the control). Scale bar: 100 μm. *P < 0.05, **P < 0.01, ***P < 0.001, ****P < 0.0001, indicate statistical difference compared to model group or between groups. ns indicates no statistical significance. (For interpretation of the references to colour in this figure legend, the reader is referred to the web version of this article.)

demonstrated that CHALT exerted anti-psoriasis properties by suppressing IL-6 expression and IL-6 related inflammation.

STAT3 signaling pathway plays crucial roles in the pathogenesis of psoriasis, and STAT3 blockade could attenuate inflammation and thus serve as a strategy for treating psoriasis. We have shown that CHALT could restrain the phosphorylation of STAT3 and src (Fig. 4G), thereby exerting anti-psoriasis properties *in vitro*. We also tested the phosphorylation of STAT as well as the upstream proteins (src and JAK2) *in vivo* psoriatic lesions using immunoblot assay [7,52,53]. As shown in Fig. 7E, IMQ exposure upregulated the expression of p-STAT3, p-src, and p-JAK2 compared to the normal mice, which could be downregulated by ALT or CHALT, and 30 μM CHALT exerted the toughest inhibition, even though no effect was observed on total STAT3 expression. 30 μM ALT and 20 μM CHALT also showed an inhibitory effect, but not sufficient. The quantitative analysis was corresponding to the blots (Fig. 7F-7H). The deactivation of STAT3 signaling also contributed to the decreased IL-6 expression. These results were consistent with the *in vitro* data, demonstrating that CHALT could exert a superior anti-psoriasis effect by inhibiting STAT3 activation. It should be mentioned is that although STAT3 blocking does not act on Th17 cells directly, it blocks the upstream IL-23 and thereby decreases the Th17 cell differentiation and cytokine release [7,54].

As the biggest immune organ, the spleen harbors various types of immune cells and plays an important role in immune function. The immune system is usually activated in psoriatic patients, whose spleen is often enlarged. We recorded the appearance and measured the spleen size after different treatments. As shown in Fig. 8A, the spleen in model group was enlarged compared to that in the normal group, and the spleen/body ratio (wt%) increased more than 3 folds (Fig. 8B), indicating the increased cell number in spleen and immune activation. ALT and CHALT treatment decreased the spleen size, and 30 μM CHALT presented the lowest spleen/body ratio, indicating the best treatment outcome. 30 μM ALT and 20 μM CHALT did not have a statistical difference, which was in agreement with the above results, also suggesting that CH nanoparticle loading strength the therapeutical efficacy of ALT. These results depicted that CHALT could exert an immunomodulation function in the application of psoriasis treatment. Based on this, we further

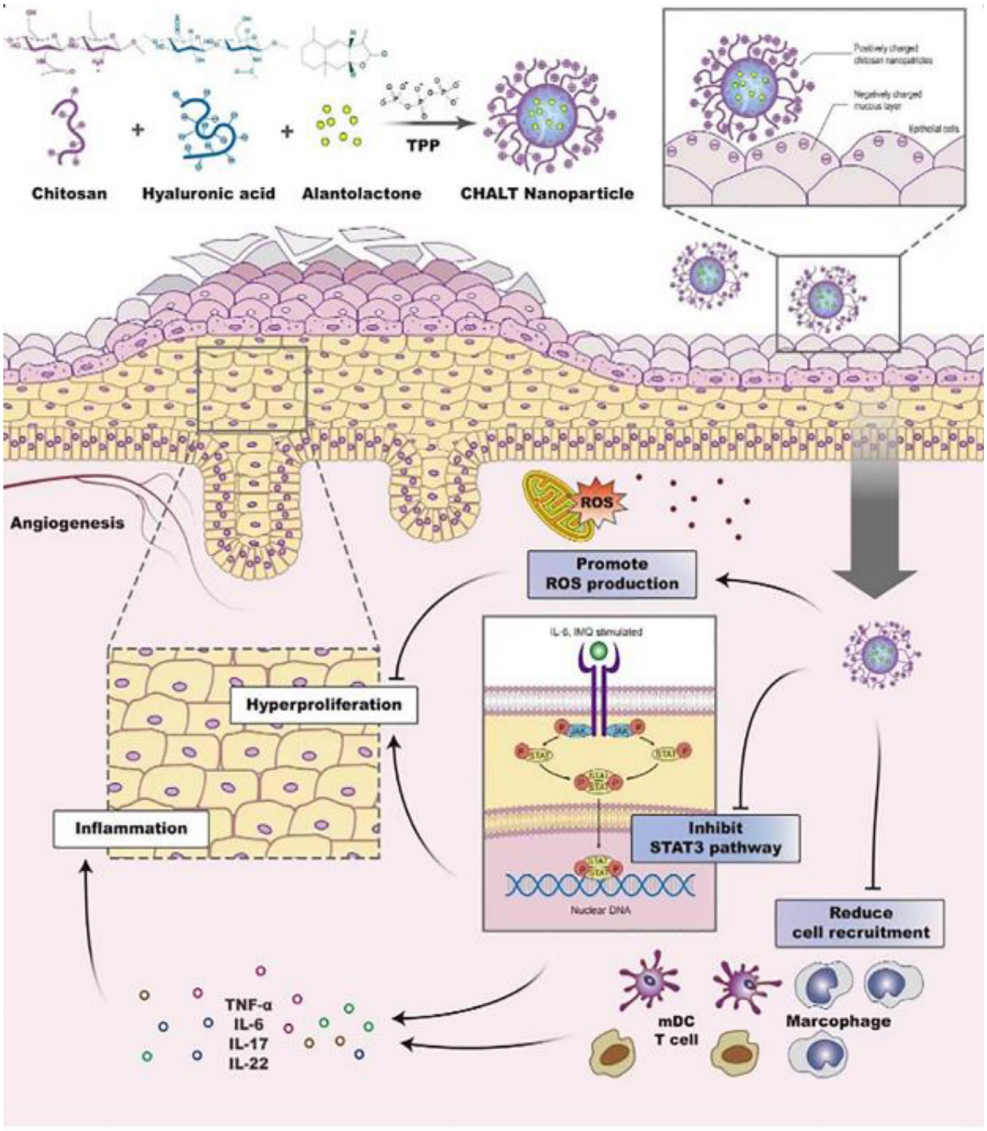

Scheme 1 – Alantolactone-loaded nanoparticle (CHALT) suppress psoriasis by inhibiting STAT3 pathway and restricting immune cell recruitment.

detected the T cell infiltration in psoriatic skin lesions using immunofluorescence assay. As shown in Fig. 8C-8F, we monitored the presentation of $CD4^+$ and $CD8^+$ cells in skin tissue after various treatments. The skin in model group recruited plenty of $CD4^+$ and $CD8^+$ cells in psoriatic skin lesions, more than 40 folds compared to the normal group. CHALT and ALT reduced the infiltration of $CD4^+$ and $CD8^+$ cells in skin tissue, and 30 μM CHALT presented the best effect. 30 μM ALT and 20 μM CHALT showed similar results, consistent with the spleen/body ratio data. The suppressed activation of the immune system also contributed to the decreased infiltration of T cells in skin. In addition, it has been reported that ALT could induce cell death in Leukemia T cells [55], which might also be related to the decreased T cell infiltration in the skins after ALT or CHALT treatment. These results suggested that CHALT could modulate systemic immune reaction and decrease T cell infiltration in psoriatic skin lesions Scheme 1.

4. Conclusion

In this study, we developed and characterized ALT-loaded chitosan/hyaluronic acid nanoparticles (CHALT), and investigated its therapeutic potential for psoriasis treatment by topical application. CHALT effectively abrogated the keratocyte hyperproliferation by inducing ROS-mediated apoptosis with loss of mitochondrial membrane potential, and also inhibited IL-6-induced STAT3 signaling activation and inflammatory reaction in the HaCaT cell line. In an IMQ-induced psoriasis model, the topical treatment with CHALT effectively ameliorated the symptoms of psoriasis by abrogating epidermal hyperproliferation, suppressing angiogenesis, attenuating the STAT3 hyperactivation and related inflammation, and modulating systemic immune reaction. CHALT showed limited systemic toxicity, evidenced by the neglectable weight changes. In summary, CHALT

offered a promising STAT3-inhibitor-based formulation for psoriasis therapy by topical application.

Conflicts of interest

The authors declare no conflict of interest.

Acknowledgement

This research was financially supported by the National Natural Science Foundation of China (81903551), Zhejiang Province Natural Science Foundation (LQ19H300001) and Excellent Young Scientist Training Program fund from Wenzhou Medical University.

Supplementary materials

Supplementary material associated with this article can be found, in the online version, at doi:10.1016/j.ajps.2022.02.003.

REFERENCES

[1] Grozdev I, Korman N, Tsankov N. Psoriasis as a systemic disease. Clin Dermatol 2014;32:343–50.
[2] Gonzalez-Parra S, Dauden E. Psoriasis and depression: the role of inflammation. Actas Dermosifiliogr 2019;110:12–19.
[3] Boehncke WH, Psoriasis Schön MP. Lancet North Am Ed 2015;386:983–94.
[4] Psoriasis Lebwohl M. Ann Intern Med 2018;168 Itc49-64.
[5] Masson W, Lobo M, Molinero G. Psoriasis and cardiovascular risk: a comprehensive review. Adv Ther 2020;37:2017–33.
[6] Armstrong AW, Read C. Pathophysiology, clinical presentation, and treatment of psoriasis: a a review. JAMA 2020;323:1945–60.
[7] Calautti E, Avalle L, Poli V. Psoriasis: A STAT3-Centric view. Int J Mol Sci 2018:19.
[8] Wang A, Wei J, Lu C, Chen H, Zhong X, Lu Y, et al. Genistein suppresses psoriasis-related inflammation through a STAT3–NF-κB-dependent mechanism in keratinocytes. Int Immunopharmacol 2019;69:270–8.
[9] Gennari A, Rios de la Rosa JM, Hohn E, Pelliccia M, Lallana E, Donno R, et al. The different ways to chitosan/hyaluronic acid nanoparticles: templated vs direct complexation. Influence of particle preparation on morphology, cell uptake and silencing efficiency. Beilstein J Nanotechnol 2019;10:2594–608.
[10] Andres RM, Hald A, Johansen C, Kragballe K, Iversen L. Studies of Jak/STAT3 expression and signalling in psoriasis identifies STAT3-Ser727 phosphorylation as a modulator of transcriptional activity. Exp Dermatol 2013;22:323–8.
[11] Sano S, Chan KS, Carbajal S, Clifford J, Peavey M, Kiguchi K, et al. Stat3 links activated keratinocytes and immunocytes required for development of psoriasis in a novel transgenic mouse model. Nat Med 2005;11:43–9.
[12] Yuan X, Li N, Zhang M, Lu C, Du Z, Zhu W, et al. Taxifolin attenuates IMQ-induced murine psoriasis-like dermatitis by regulating T helper cell responses via Notch1 and JAK2/STAT3 signal pathways. Biomed Pharmacother 2020;123:109747.
[13] Thatikonda S, Pooladanda V, Sigalapalli DK, Godugu C. Piperlongumine regulates epigenetic modulation and alleviates psoriasis-like skin inflammation via inhibition of hyperproliferation and inflammation. Cell Death Dis 2020;11:21.
[14] Agerholm R, Rizk J, Vinals MT, Bekiaris V. STAT3 but not STAT4 is critical for gammadeltaT17 cell responses and skin inflammation. EMBO Rep 2019;20:e48647.
[15] Heirich PC, Behrmann I, Müller-Newen G, Schaper F, Graeve L. Interleukin-6-type cytokine signalling through the gp130 Jak STAT pathway. Biochem J 1998;334:297–314.
[16] Wolk K, Haugen HS, Xu W, Witte E, Waggie K, Anderson M, et al. IL-22 and IL-20 are key mediators of the epidermal alterations in psoriasis while IL-17 and IFN-gamma are not. J Mol Med (Berl) 2009;87:523–36.
[17] Bao S, Zheng H, Ye J, Huang H, Zhou B, Yao Q, et al. Dual targeting EGFR and STAT3 with erlotinib and alantolactone co-loaded PLGA nanoparticles for pancreatic cancer treatment. Front Pharmacol 2021;12:625084.
[18] Jiang X, Yao Q, Xia X, Tang Y, Sun M, Li Y, et al. Self-assembled nanoparticles with bilirubin/JPH203 alleviate imiquimod-induced psoriasis by reducing oxidative stress and suppressing Th17 expansion. Chem Eng J 2022;431:133956.
[19] Yao Q, Kou L, Tu Y, Zhu L. MMP-responsive 'smart' drug delivery and tumor targeting. Trends Pharmacol Sci 2018;39:766–81.
[20] Jing Q, Ruan H, Li J, Wang Z, Pei L, Hu H, et al. Keratinocyte membrane-mediated nanodelivery system with dissolving microneedles for targeted therapy of skin diseases. Biomaterials 2021;278:121142.
[21] Pukale SS, Sharma S, Dalela M, Singh AK, Mohanty S, Mittal A, et al. Multi-component clobetasol-loaded monolithic lipid-polymer hybrid nanoparticles ameliorate imiquimod-induced psoriasis-like skin inflammation in Swiss albino mice. Acta Biomater 2020;115:393–409.
[22] Quan XQ, Kang L, Yin XZ, Jin ZH, Gao ZG. Synthesis of PEGylated hyaluronic acid for loading dichloro(1,2-diaminocyclohexane)platinum(II) (DACHPt) in nanoparticles for cancer treatment. Chin Chem Lett 2015;26:695–9.
[23] Huang ZW, Shi Y, Zhai YY, Du CC, Zhai J, Yu RJ, et al. Hyaluronic acid coated bilirubin nanoparticles attenuate ischemia reperfusion-induced acute kidney injury. J Control Release 2021;334:275–89.
[24] Zhang Y, Xia Q, Li Y, He Z, Li Z, Guo T, et al. CD44 assists the topical anti-psoriatic efficacy of curcumin-loaded hyaluronan-modified ethosomes: a new strategy for clustering drug in inflammatory skin. Theranostics 2019;9:48–64.
[25] Liang H, Yan Y, Wu J, Ge X, Wei L, Liu L, et al. Topical nanoparticles interfering with the DNA-LL37 complex to alleviate psoriatic inflammation in mice and monkeys. Sci Adv 2020;6:eabb5274.
[26] Muanprasat C, Chatsudthipong V. Chitosan oligosaccharide: Biological activities and potential therapeutic applications. Pharmacol Ther 2017;170:80–97.
[27] Shaker DS, Ishak RAH, Ghoneim A, Elhuoni MA. Nanoemulsion: a review on mechanisms for the transdermal delivery of hydrophobic and hydrophilic drugs. Sci Pharm 2019;87.
[28] Qiu B, Gong M, He QT, Zhou PH. Controlled release of interleukin-1 receptor antagonist from hyaluronic acid-chitosan microspheres attenuates interleukin-1beta-Induced inflammation and apoptosis in chondrocytes. Biomed Res Int 2016;2016:6290957.
[29] Kou L, Sun R, Xiao S, Zheng Y, Chen Z, Cai A, et al. Ambidextrous approach to disrupt redox balance in tumor cells with increased ROS production and decreased GSH synthesis for cancer therapy. ACS Appl Mater Interfaces 2019;11:26722–30.

[30] Kou L, Sun R, Jiang X, Lin X, Huang H, Bao S, et al. Tumor microenvironment-responsive, multistaged liposome induces apoptosis and ferroptosis by amplifying oxidative stress for enhanced cancer therapy. ACS Appl Mater Interfaces 2020;12:30031–43.
[31] Kou L, Jiang X, Tang Y, Xia X, Li Y, Cai A, et al. Resetting amino acid metabolism of cancer cells by ATB0,+-targeted nanoparticles for enhanced anticancer therapy. Bioactive materials 2022;9:15–28.
[32] Luesakul U, Puthong S, Sansanaphongpricha K, Muangsin N. Quaternized chitosan-coated nanoemulsions: A novel platform for improving the stability, anti-inflammatory, anti-cancer and transdermal properties of Plai extract. Carbohydr Polym 2020;230:115625.
[33] Kou L, Sun J, Zhai Y, He Z. The endocytosis and intracellular fate of nanomedicines: implication for rational design. Asian J Pharm Sci 2013;8:1–10.
[34] Wang X, Lu X, Zhu R, Zhang K, Li S, Chen Z, et al. Betulinic acid induces apoptosis in differentiated PC12 cells via ROS-mediated mitochondrial pathway. Neurochem Res 2017;42:1130–40.
[35] B Mignotte 1 JLV. Mitochondria and apoptosis. Eur J Biochem 1998:1–15.
[36] Miao X, Xiang YW, Mao WW, Chen YR, Li Q, Fan B. TRIM27 promotes IL-6-induced proliferation and inflammation factor production by activating STAT3 signaling in HaCaT cells. Am J Physiol Cell Physiol 2019:272–81.
[37] Goodman WA, Levine AD, Massari JV, Sugiyama H, McCormick TS, Cooper KD. IL-6 signaling in psoriasis prevents immune suppression by regulatory T cells. J Immunol 2009;183:3170–6.
[38] Zampetti A. Proinflammatory cytokine production in HaCaT cells treated by eosin:implications for the topical treatment of psoriasis. Int J Immunopathol Pharmacol 2009:1067–75.
[39] Lu X, Luo F, Liu Y, Zhang A, Li J, Wang B, et al. The IL-6/STAT3 pathway via miR-21 is involved in the neoplastic and metastatic properties of arsenite-transformed human keratinocytes. Toxicol Lett 2015;237:191–9.
[40] Chun J, Li RJ, Cheng MS, Kim YS. Alantolactone selectively suppresses STAT3 activation and exhibits potent anticancer activity in MDA-MB-231 cells. Cancer Lett 2015;357:393–403.
[41] Zheng H, Yang L, Kang Y, Chen M, Lin S, Xiang Y, et al. Alantolactone sensitizes human pancreatic cancer cells to EGFR inhibitors through the inhibition of STAT3 signaling. Mol Carcinog 2019;58:565–76.
[42] Maryam A, Mehmood T, Zhang H, Li Y, Khan M, Ma T. Alantolactone induces apoptosis, promotes STAT3 glutathionylation and enhances chemosensitivity of A549 lung adenocarcinoma cells to doxorubicin via oxidative stress. Sci Rep 2017;7:6242.
[43] Khan M, Li T, Ahmad Khan MK, Rasul A, Nawaz F, Sun M, et al. Alantolactone induces apoptosis in HepG2 cells through GSH depletion, inhibition of STAT3 activation, and mitochondrial dysfunction. Biomed Res Int 2013;2013:719858.
[44] Keum H, Kim TW, Kim Y, Seo C, Son Y, Kim J, et al. Bilirubin nanomedicine alleviates psoriatic skin inflammation by reducing oxidative stress and suppressing pathogenic signaling. J Control Release 2020;325:359–69.
[45] Wang X, Ren R, Xu Z, Huang H, Jiang W, Ma J. Tirbanibulin attenuates pulmonary fibrosis by modulating Src/STAT3 signaling. Frontiers in pharmacology 2021;12:693906.
[46] Swindell WR, Michaels KA, Sutter AJ, Diaconu D, Fritz Y, Xing X, et al. Imiquimod has strain-dependent effects in mice and does not uniquely model human psoriasis. Genome Med 2017;9:24.
[47] Elshabrawy HA, Chen Z, Volin MV, Ravella S, Virupannavar S, Shahrara S. The pathogenic role of angiogenesis in rheumatoid arthritis. Angiogenesis 2015;18:433–48.
[48] Afonina IS, Van Nuffel E, Beyaert R. Immune responses and therapeutic options in psoriasis. Cell Mol Life Sci 2021;78:2709–27.
[49] Cao GY, O'Brien CD, Zhou Z, Sanders SM, Greenbaum JN, Makrigiannakis A, et al. Involvement of human PECAM-1 in angiogenesis and in vitro endothelial cell migration. Am J Physiol Cell Physiol 2002:1181–90.
[50] Wu Y, Liu L, Bian C, Diao Q, Nisar MF, Jiang X, et al. MicroRNA let-7b inhibits keratinocyte differentiation by targeting IL-6 mediated ERK signaling in psoriasis. Cell Commun Signal 2018;16:58.
[51] Saggini A, Chimenti S, Chiricozzi A. IL-6 as a druggable target in psoriasis: focus on pustular variants. J Immunol Res 2014;2014:964069.
[52] Bhummaphan N, Petpiroon N, Prakhongcheep O, Sritularak B, Chanvorachote P. Lusianthridin targeting of lung cancer stem cells via Src-STAT3 suppression. Phytomedicine 2019;62:152932.
[53] Bian G, Wang L, Xie Q, Wang Y, Feng H, Yu Y, et al. DGT, a novel heterocyclic diterpenoid, effectively suppresses psoriasis via inhibition of STAT3 phosphorylation. Br J Pharmacol 2021;178:636–53.
[54] Han F, Guo H, Wang L, Zhang Y, Sun L, Dai C, et al. TSLP produced by aspergillus fumigatus-stimulated DCs promotes a Th17 response through the JAK/STAT signaling pathway in fungal keratitis. Invest Ophthalmol Vis Sci 2020;61:24.
[55] Dirsch VM SH, Vollmar AM. Cytotoxic sesquiterpene lactones mediate their death-inducing effect in leukemia T cells by triggering apoptosis. Planta Med 2001:557–9.